Physica B: Condensed Matter 531 (2018) 64–69

Contents lists available at ScienceDirect

Physica B: Condensed Matter

journal homepage: www.elsevier.com/locate/physb

Tensile behavior of $Cu_{50}Zr_{50}$ metallic glass nanowire with a B2 crystalline precipitate

Matias Sepulveda-Macias [a,*], Nicolas Amigo [a,b], Gonzalo Gutierrez [a]

[a] Grupo de NanoMateriales, Departamento de Física, Facultad de Ciencias, Universidad de Chile, Casilla 653, Santiago, Chile
[b] Departamento de Ingeniería Mecánica, Facultad de Ciencias Físicas y Matemáticas, Universidad de Chile, Santiago, Chile

ARTICLE INFO

Keywords:
Nanowires
Metallic glasses
Precipitate
Tensile test
Molecular dynamics simulation

ABSTRACT

A molecular dynamics study of the effect of a single B2–CuZr precipitate on the mechanical properties of $Cu_{50}Zr_{50}$ metallic glass nanowires is presented. Four different samples are considered: three with a 2, 4 and 6 nm radii precipitate and a precipitate-free sample. These systems are submitted to uniaxial tensile test up to 25% of strain. The interface region between the precipitate and the glass matrix has high local atomic shear strain, activating shear transformation zones, which concentrates in the neighborhood of the precipitate. The plastic regime is dominated by necking, and no localized shear band is observed for the samples with a 4 and 6 nm radii precipitate. In addition, the yield stress decreases as the size of the precipitate increases. Regarding the precipitate structure, no martensitic phase transformation is observed, since neither the shear band hit the precipitate nor the stress provided by the tensile test is enough to initiate the transformation. It is concluded that, in contrast to the case when multiple precipitates are present in the sample, a single precipitate concentrates the shear strain around its surface, eventually causing the failure of the nanowire.

1. Introduction

Metallic glasses (MGs) are metallic alloys that have an amorphous structure, and because of that, they possess unique properties. For instance, bulk metallic glasses (BMGs) have high yield strength and corrosion resistance, high magnetic permeability, very low coercivity, and they even are resistant against radiation damage, among others [1–6]. Due to their excellent mechanical, physical and chemical properties, MGs have great potential for structural and functional applications [7–10]. When the size of MGs decrease, new properties arises, as is the case of MG nanowires.

Nanowires, both crystalline and amorphous, have an increasing importance in recent years, since they play a key role in the future generation of nanodevices, ranging from microelectronics to biomedicine to electrochemistry [11]. Hence, it is of fundamental interest to understand the mechanical behavior and how they differ from their bulk counterparts. In this sense, from a basic point of view, they are an ideal test–bed in order to understand how the properties of the material changes when the size of the sample decreases. Particularly, MG nanowires present less limitations than crystalline nanowires for the preparation and practical applications [12].

Interestingly, while the Achille's heel of BMGs is the limited ductility and immediate fracture when they are subjected to mechanical test [13], MG nanowires present a much more complex mechanical behavior. In fact, depending on their preparation, the aspect ratio and the mechanical test (tensile/compressive), among others, they exhibit strengthening or weakening [14–16]. For instance, to explain the ductility of some nanowires, it has been argued that when the volume of a metallic glass sample decreases, the elastic energy stored decreases faster than the surface energy of the region associated with the localized shear, making the process of formation of shear bands (SBs) slower and less violent, avoiding a catastrophic rupture of the material [17,18]. Regarding the preparation procedure, the MG nanowires may have different structure and chemical concentration. In particular it is interesting to explore the effect of precipitates in the sample. Hence, some of the following questions arise: What are the changes in the mechanical properties when a crystalline phase is included? It has been observed that precipitates increase the ductility of BMGs. The explanation given by Albe *et al.* [19] for $Cu_{64}Zr_{36}$ metallic glass with Cu precipitates is that shear events start at the interface between the glass and the precipitates, thus promoting the formation of shear transformation zones (STZs) and then acting as nucleation sites for SBs. Moreover, at the same

* Corresponding author.
E-mail addresses: msepmacias@gmail.com (M. Sepulveda-Macias), nico.amigo.a@gmail.com (N. Amigo), gonzalogutierrez@uchile.cl (G. Gutierrez).

https://doi.org/10.1016/j.physb.2017.12.005
Received 17 October 2017; Received in revised form 24 November 2017; Accepted 1 December 2017
Available online 5 December 2017

time when the BMG is strained, the precipitate suffers plastic deformation. In the case of MG nanowires, if a B2–CuZr precipitate is considered, does it undergo a martensitic phase transformation as indicated by Sutrakar *et al.* [20]? These are some of the questions that we want to address in this work. Here we present a molecular dynamic study which shows the effects of spherical crystalline B2–CuZr precipitate on the mechanical properties, including the formation of SBs in $Cu_{50}Zr_{50}$ metallic glass nanowires under uniaxial tensile test. The local structure of atoms is analyzed in detail by means of the local atomic shear strain. This article is organized as follows: In Sec. 2 we explain the simulation procedure, the interatomic potential and tools employed. In Sec. 3 we present the results of this work and finally in Sec. 4 we draw the conclusions.

2. Methodology

The first step towards simulating CuZr metallic glass nanowires using molecular dynamics simulations, is the choice of an appropriate interatomic potential to accurately describe the lattice parameters, melting temperatures, formation energies, among other properties. Hence, we adopt a commonly accepted Finnis–Sinclair type embedded atom method (EAM) proposed by Mendelev *et al.* for CuZr systems [21] since it has been widely used and accepted when studying CuZr metallic glasses and the B2–CuZr phase [20,22].

In order to prepare the $Cu_{50}Zr_{50}$ metallic glass, we adopt a similar procedure as the one proposed by Wang *et al.* [23]. First of all, a B2–CuZr system with dimensions of $L_x \times L_y \times L_z = 9.07 \times 3.88 \times 3.88\ \text{nm}^3$, composed of 8064 atoms is created, where periodic boundary conditions (PBC) are set in all three directions. The temperature and pressure are fixed at 2000 K and 0 GPa respectively, allowing the system to relax for 2 ns using the NPT ensemble [24]. The integration timestep is set at 1 fs. Then, the system is cooled down to 300 K in the same way as is detailed in our previous work [25]. Thus, the calculated cooling rate is 5×10^{10} K/s.

With the procedure described above, a $Cu_{50}Zr_{50}$ metallic glass system composed of 8064 atoms is obtained. The next step consists of replicating the system five times in each direction in order to generate the nanowire, giving a total of 1 million atoms with dimensions of $L_x \times L_y \times L_z = 45.36 \times 19.44 \times 19.44\ \text{nm}^3$. Free boundary conditions are set in y and z directions, and PBC are kept in the axial direction. At this point, a spherical crystalline B2–CuZr precipitate, with radius $r = 2, 4, 6$ nm, is embedded at the center of the system. This is done by removing a sphere of radius $r + \Delta r$ from the glass matrix, where r is the radius of the precipitate and $\Delta r = 2.5$ Å is added in order to avoid overlapping atoms between both phase. Then, the precipitate, with radius r, is embedded into the bulk, where the [100] direction is along the tensile loading. The volume fraction of the crystalline phase related to the total composite volume is from ~0.1% to ~5.2%. This new configuration is allowed to relax for 100 ps in the NVT ensemble, at 300 K, to ensure a well–equilibrated sample. In Fig. 1 we present a half of the system which corresponds to a cut at the middle of the sample. This cross–section shows the interface between the precipitate and the metallic glass matrix after relaxation. It can be distinguished three regions. The atoms in region 1 are ordered in the B2 phase. Atoms in region 2 belong to the interface, where it is seen a transition from crystalline to amorphous structure. Finally, in region 3 we observe a fully amorphous phase.

The tensile test is performed by loading the axial direction of the system at a strain rate of $5 \times 10^8\ \text{s}^{-1}$. For this purpose, the positions of the atoms are rescaled each time step. The temperature is kept constant at 300 K, in the NVT ensemble, during the whole procedure. The molecular dynamics simulation is carried out using the classical molecular dynamics code LAMMPS [26].

In order to analyse our simulation, we use several diagnostic tools. For stress–strain curve, we evaluate the σ_{xx} component of the stress tensor, as well as the axial component of the strain tensor, denoted as ε.

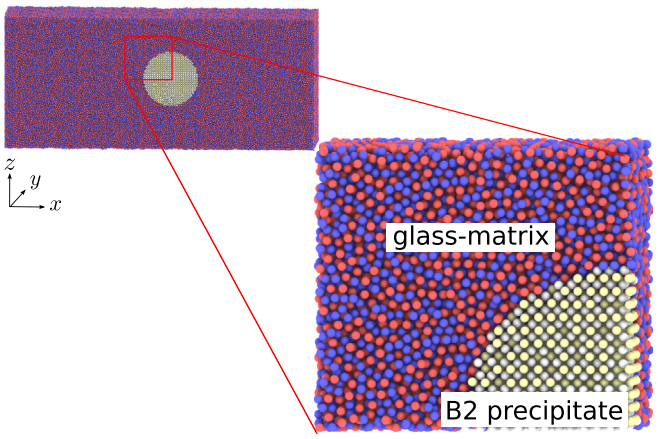

Fig. 1. Cross-section view of the sample showing the interface between the precipitate and the metallic glass matrix after relaxation.

To quantify the structural changes of the sample at atomic–scale we use, pair distribution function (PDF), the common neighbor analysis (CNA) and the local atomic shear strain η^{Mises} [27]. This parameter requires two atomic configurations, the current and the reference one. The first step is to seek a local affine transformation $\mathbf{J}_i$ that best map

$$\{\mathbf{d}_{ji}^0\} \rightarrow \{\mathbf{d}_{ji}\}, \quad \forall j \in N_i^0, \tag{1}$$

where $\mathbf{d}$ are vector separations between atom i and each neighbor j. Here the superscript 0 stands for reference configuration, and N_i^0 is the number of neighbors of atom i at the reference configuration. Then, we seek $\mathbf{J}_i$ that minimizes

$$\sum_{j \in N_i^0} \left| \mathbf{d}_{ji}^0 \mathbf{J}_i - \mathbf{d}_{ji} \right|^2 \rightarrow \mathbf{J}_i = \left(\sum_{j \in N_i^0} \mathbf{d}_{ji}^{0T} \mathbf{d}_{ji}^0 \right)^{-1} \left(\sum_{j \in N_i^0} \mathbf{d}_{ji}^{0T} \mathbf{d}_{ji} \right). \tag{2}$$

With $\mathbf{J}_i$, the Lagrangian strain matrix can be calculated as

$$\eta_i = \frac{1}{2} \left(\mathbf{J}_i \mathbf{J}_i^T - \mathbf{I} \right), \tag{3}$$

where we can define the local shear invariant for atom i as

$$\eta_i^{\text{Mises}} = \sqrt{\eta_{yz}^2 + \eta_{xz}^2 + \eta_{xy}^2 + \frac{(\eta_{yy} - \eta_{zz})^2 + (\eta_{xx} - \eta_{zz})^2 + (\eta_{xx} - \eta_{yy})^2}{6}}, \tag{4}$$

where $\eta_{\alpha\beta}$ are the components of the strain tensor of atom i. We visualize η_i^{Mises} using the software OVITO [28].

3. Results

3.1. Effect of the precipitate in the stress–strain curve

We determine the stress–strain curves for the three systems and compare them to the precipitate–free case [25]. In Fig. 2 we observe that all of them present an elastic behavior up to 4%, an homogeneous deformation zone between 4% and 6%, and beyond 6% an inhomogeneous strain zone. The Young's modulus E and yield stress σ_y (obtained as the peak stress) of each curve are summarized in Table 1. It is observed that the presence of the precipitate slightly modifies the Young's modulus of the glass matrix. On the other hand, the yield stress decreases according to the precipitate size, which is shown in the inset of Fig. 2. The rationale behind this fact is as follow: with a bigger size, the interface area between the B2–CuZr phase and the glass matrix increases. Thus, there is more internal stress at the interface, promoting the plastic regime of the sample by means of STZs.

To characterize the structure of the precipitate in our cases, we calculate their pair distribution function (PDF). The results are displayed

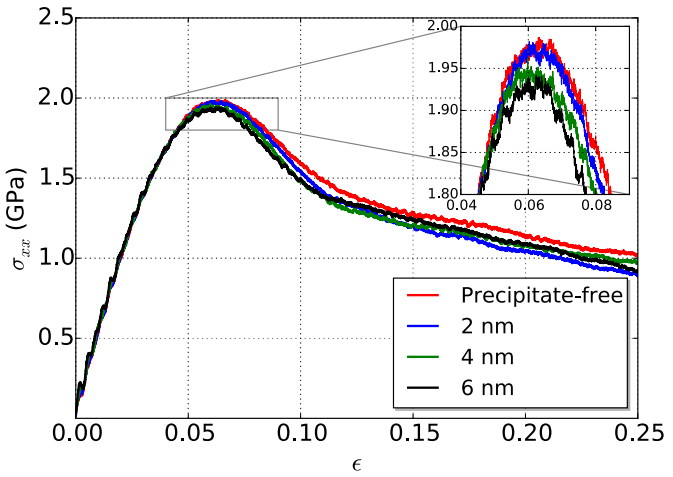

Fig. 2. The stress–strain curves for the $Cu_{50}Zr_{50}$ metallic glass with crystalline B2–CuZr phase under tensile deformation. The inset shows the decrease of the yield stress with the increase of the size of the precipitate.

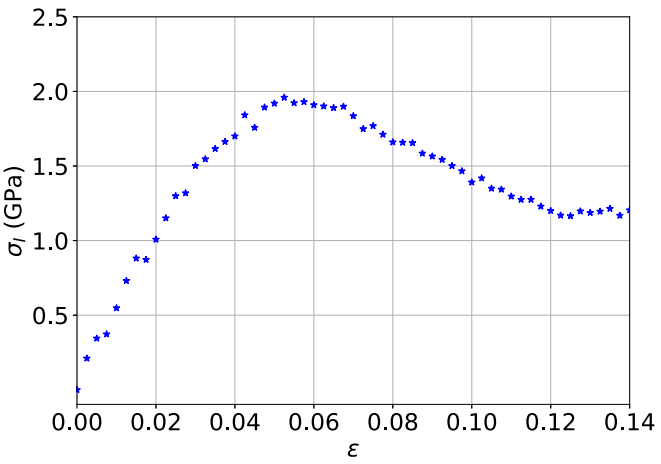

Fig. 4. Stress, σ_I, of the precipitate ($r = 6$ nm) according to the strain of the sample. The maximum, ~2 GPa, is far below the stress needed for the martensitic transformation.

Table 1
Young's modulus E and yield stress σ_y of the $Cu_{50}Zr_{50}$ metallic glass with the crystalline B2–CuZr phase.

r (nm)	E (GPa)	σ_y (GPa)
0	56.01	1.987
2	55.72	1.978
4	55.84	1.949
6	55.13	1.932

in Fig. 3, where is observed that no significant change occurs. A further characterization was done by means of the CNA, which confirms that no transformation occurs, as it is shown in Fig. 3(d) to Fig. 3(e). Experimental studies [29–31] of CuZr–based metallic glass composites with a B2 phase report that these systems exhibit martensitic phase transformation and pseudoelasticity, when the volume fraction of the B2 phase is 40 – 80%. Interestingly, previous numerical studies shows, on one hand, that shear bands nucleate from the precipitates, which propagate and impact on other precipitates initiating the martensitic phase transformation of the B2 phase [32]. On the other, Brink *et al.* [33] analyzed the hit of a single SB on a B2–CuZr precipitate, not observing martensitic transformation of the B2 phase, arguing that the stress provided by the shear band was not enough to initiate the transformation. Like in the case of Brink [33], we also did not observe a martensitic transition. In our case, the reasons are the following. Firstly, STZs are activated at the interface, concentrating in the neighborhood of the precipitate, and no SB hits the crystalline phase. Secondly, the stress provided to the B2 phase by the tensile test is not enough to trigger the martensitic transformation. Fig. 4 shows the stress on the precipitate ($r = 6$ nm), σ_I, due to the tensile test on the whole sample. It is observed that the maximum stress is ~2.0 GPa, far below the ~12–15 GPa needed for the phase transformation indicated by Sutrakar *et al.* [20] and recent work by Amigo *et al.* [34]. In addition, Brink *et al.* [33] demonstrated that the stacking fault energy in fcc copper is overestimated by the potential of Mendelev *et al.* [35]. Thus, the stacking fault energy of the B2–CuZr system could also be overestimated, which ultimately affects the onset of the martensitic transformation [36]. It is interesting to note that the Young's modulus is 49.17 GPa, lower than the one of the glass matrix. This explains the decrease of the elastic modulus in the composites, as reported in Table 1.

3.2. Size of the precipitate and shear transformation zones activation

We have shown that the B2–CuZr precipitate does not undergo martensitic transformation. However, at the same time, as it has been

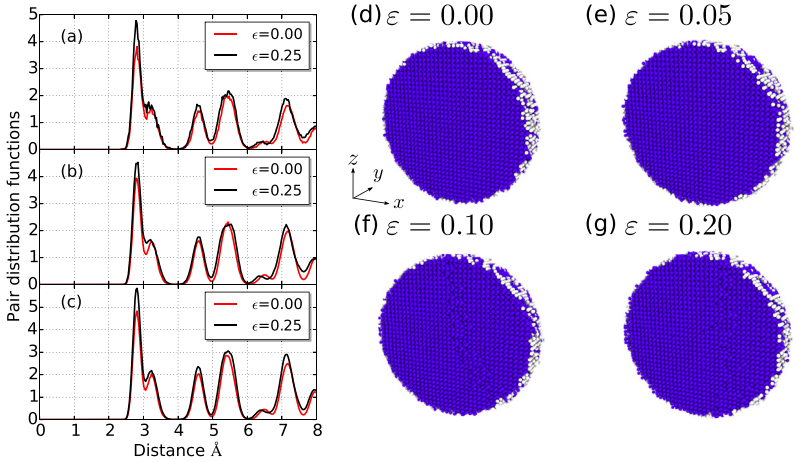

Fig. 3. Calculated pair distribution function for atoms in crystalline B2–CuZr phase. In (a) we present the situation for 2 nm radii. (b) and (c) for 4 and 6 nm radii precipitate, respectively. In the right panel from (d) to (g) the calculated common neighbor analysis for the 6 nm precipitate at different stages.

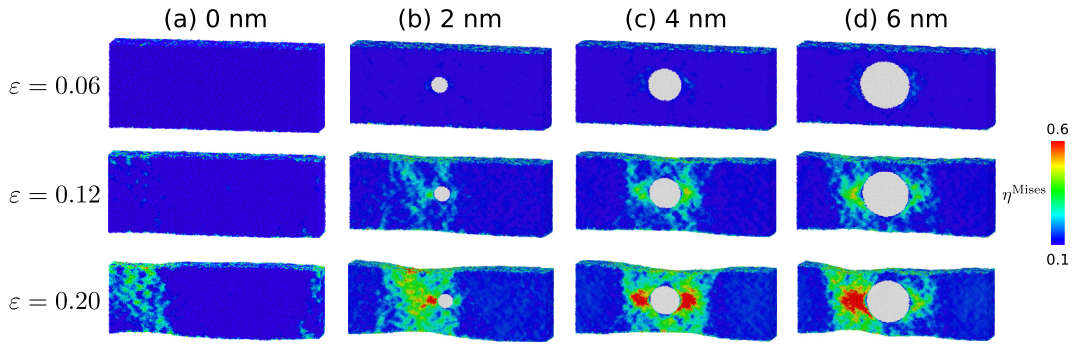

Fig. 5. Cross–section view of the $Cu_{50}Zr_{50}$ system at different stages of the simulation. From left to right the precipitate–free case reported in Ref. [25], 2, 4 and 6 nm radii precipitates respectively. Atoms are colored according to the shear strain and crystalline B2–CuZr phase is colored white. (For interpretation of the references to colour in this figure legend, the reader is referred to the web version of this article.)

already discussed in the literature, the yield stress of the whole sample decreases since the interface between the precipitate and the glass matrix promotes STZs [19,31]. In our case, it is also observed that the greater the size of the precipitate, the lower the yield stress. In the following, we will give an atomic level description of the role of the size of the precipitate in both, the STZs activation and the plastic flow of the samples.

In Fig. 5, we present the process of the STZs activation for the three radii under study, and the precipitate–free case reported in Ref. [25]. At 6–12% of the applied strain is observed that there are STZs that begin to coalesce at the crystalline–amorphous interface. This phenomenon increases for the biggest precipitate size, in good agreement with recent experimental evidences [31] revealing that the B2 phase promotes the density of the stress concentration sites. Nevertheless, in contrast with Wu observations [31], no formation and interaction of multiple shear band is seen, due to the absence of other precipitates. Note that the SB formation is delayed for the case of the precipitate–free sample, see Fig. 5(a). It is observed that Fig. 5(b) has a similar behavior, showing the formation of a single SB close to the precipitate, while in Fig. 5(c) and (d) the STZs concentrate in the neighborhood of the precipitate, but no localized SB is observed. In all four cases, the plastic flow is dominated by necking. This is clearly seen in Fig. 5, at 20% of strain. At the end, high local atomic shear strain zones are concentrated around the precipitate, eventually causing the failure of the sample.

Fig. 6 shows in detail the atoms that surround the precipitate. For our simulations, atoms with low atomic shear strain (dark blue) tend to agglomerate in high–density regions of diameter about 1.5 – 3 nm, similar to the ones reported in recent experimental and simulation works (see, for instance, Fig. 1 of Feng *et al* [37]). As it can be seen, these regions are surrounded by atoms with high local atomic shear strain that are spatially connected. In fact, they form an interconnected network, in the scale of 1 – 2 nm, which define a medium range order [38,39]. Feng *et al.* [37] argue that both regions are quite different: while atoms with low η^{Mises} are densely packed clusters, the others are loosely packed, interconnecting regions with a low density. The SBs propagate easily along the loosely packed region as the strain is applied. In our case, the presence of crystalline B2–CuZr phase changes the distribution of these clusters, since the loosely packed regions grows at the interface between the amorphous and the crystalline B2–CuZr phase and it may be the reason why the STZs coalesce at the interface between the crystalline phase and the glass matrix [31]. From Fig. 6 it is clear that the presence of crystalline phase increases the formation of loosely packed clusters that promote the activation of more than one region with high concentration of STZs, in contrast to the precipitate–free case [25]. Furthermore, this explains the decrease of the yield stress of the samples as the size of the precipitate increases. This picture is reminiscent of a polycrystalline material [37], where the grains correspond to the dark blue region, as can be seen in Fig. 6(b).

To quantify the distribution of shear strain in a sample during the tensile test, we calculate the "degree of strain localization" parameter, defined by Cheng *et al.* [40] as $\psi = \sqrt{\frac{1}{N}\sum_{i=1}^{N}(\eta_i^{\text{Mises}} - \eta_{\text{ave}}^{\text{Mises}})^2}$, where $\eta_{\text{ave}}^{\text{Mises}}$ is the average of von Mises strain of all atoms and N is the total number of atoms. ψ is interpreted as follows: a larger ψ indicates larger fluctuations in the local atomic shear strain and more localized deformation modes. Fig. 7(a) shows the ψ parameter as a function of the strain for the four samples. It is observed that all cases have almost the same ψ until $\epsilon = 0.06$, and then, ψ increases as the precipitate size increases. This is in accordance with Fig. 6, where the shear strain is more homogeneously distributed in the case with $r = 2$ nm (Fig. 6(a)), as opposed to the case with $r = 6$ nm (Fig. 6(c)), where the shear strain is heavily concentrated around the precipitate. Fig. 7(b) shows the relative number of atoms with $\eta^{\text{Mises}} > 0.3$. It is observed that this number is the same in all samples until $\epsilon = 0.10$. Nevertheless, by further straining the systems, the number of atoms with $\eta^{\text{Mises}} > 0.3$ is higher when the precipitate is bigger. Hence, it is observed that a single precipitate concentrates the shear in the sample. Note, that in contrast to our results, it has been previously reported in the literature that B2–CuZr phase improves ductility of MGs [29,31,32,41]. However, those studies consider multiple regions of B2–CuZr phase. These phases undergo martensitic transformation and at the same time, several SBs are nucle-

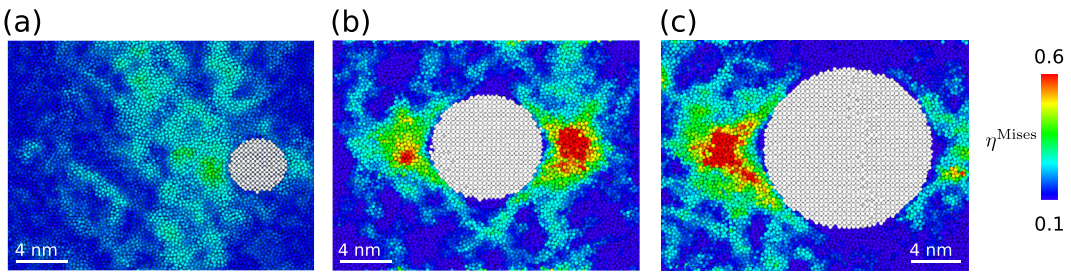

Fig. 6. Image of the structure of $Cu_{50}Zr_{50}$ with $\epsilon = 12\%$. (a), (b) and (c) stands for crystalline precipitates of 2, 4, 6 nm radii respectively.

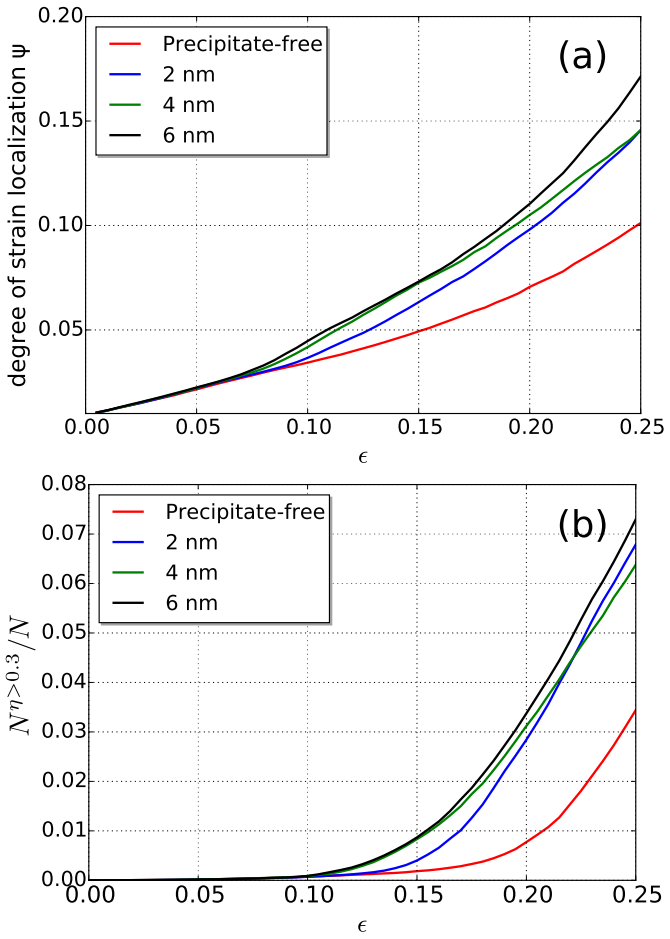

Fig. 7. (a) Degree of strain localization parameter. (b) shows the relative number of atoms with $\eta^{\text{Mises}} > 0.3$.

ated at the interfaces, enhancing the plasticity of the system. Since our simulations have a single B2–CuZr precipitate, that in addition do not show phase transformation, an inverse effect takes place, i.e. the shear strain has higher values and is more localized around the crystalline phase, which could eventually cause the failure of the nanowire.

4. Conclusions

We have presented the effect of a crystalline B2–CuZr precipitate in $Cu_{50}Zr_{50}$ metallic glass nanowires under tensile loading. According to our results, the yield stress decreases as the size of the precipitate increases, due to the bigger amount of atoms that have high local atomic shear strain at the crystalline–amorphous interface. Thus, shear transformation zones grow, but no localized shear band is observed for the samples with a 4 and 6 nm radii precipitate. Regarding the crystalline precipitate, no martensitic phase transformation is observed in all three samples, since the shear transformation zones concentrates around the precipitate, avoiding the localization of a shear band. In addition, the stress provided by the tensile test is not enough to initiate the martensitic transformation of the B2–CuZr phase. Thus, our samples do not exhibit pseudoelasticity.

In previous studies [19,32] it was observed that multiple crystalline precipitates promote the nucleation of shear bands at the crystalline–amorphous interface. These shear bands grow and propagates, interacting among them and hitting other precipitates, which undergo martensitic phase transformation, resulting in the enhancement of the plasticity of the system. In contrast, in this study we have shown that a single precipitate have a different effect: it induces the onset of STZs, that eventually coalesce, forming a shear band. However, this shear band does not localize in the sample and the plasticity is dominated by necking.

Acknowledgements

M.S-M. thanks to CONICyT Ph.D. fellowship No. 21140904. NA thanks to CONICyT PhD fellowship No. 21151448. G.G. thanks to grants PAIFAC 2016, Facultad de Ciencias, Universidad de Chile.

References

[1] W.L. Johnson, Bulk metallic glasses a new engineering material, Curr. Opin. Solid State Mater. Sci. 1 (3) (1996) 383–386, https://doi.org/10.1016/S1359-0286(96)80029-5.
[2] M. Telford, The case for bulk metallic glass, Mater. Today 7 (3) (2004) 36–43, https://doi.org/10.1016/S1369-7021(04)00124-5.
[3] W. Wang, C. Dong, C. Shek, Bulk metallic glasses, Mater. Sci. Eng. R Rep. 44 (23) (2004) 45–89, https://doi.org/10.1016/j.mser.2004.03.001.
[4] F. Breu, S. Guggenbichler, J. Wollmann, Bulk metallic glasses, Vasa 37 (July) (2008) 502–504, http://medcontent.metapress.com/index/A65RM03P4874243N.pdf.
[5] A.L. Greer, Metallic glasseson the threshold, Mater. Today 12 (12) (2009) 14–22, https://doi.org/10.1016/S1369-7021(09)70037-9.
[6] L. Zhong, J. Wang, H. Sheng, Z. Zhang, S.X. Mao, Formation of monatomic metallic glasses through ultrafast liquid quenching, Nature 512 (7513) (2014) 177–180, letter, https://doi.org/10.1038/nature13617.
[7] D.C. Hofmann, J.-Y. Suh, A. Wiest, G. Duan, M.-L. Lind, M.D. Demetriou, W.L. Johnson, Designing metallic glass matrix composites with high toughness and tensile ductility, Nature 451 (February) (2008) 1085–1089, https://doi.org/10.1038/nature06598.
[8] M.E. Launey, D.C. Hofmann, W.L. Johnson, R.O. Ritchie, Solution to the problem of the poor cyclic fatigue resistance of bulk metallic glasses, Proc. Natl. Acad. Sci. U. S. A. 106 (2009) 4986–4991, https://doi.org/10.1073/pnas.0900740106.
[9] W.H. Wang, Bulk metallic glasses with functional physical properties, Adv. Mater. 21 (45) (2009) 4524–4544, https://doi.org/10.1002/adma.200901053.
[10] S.V. Ketov, Y.H. Sun, S. Nachum, Z. Lu, A. Checchi, A.R. Beraldin, H.Y. Bai, W.H. Wang, D.V. Louzguine-Luzgin, M.A. Carpenter, A.L. Greer, Rejuvenation of metallic glasses by non-affine thermal strain, Nature 524 (7564) (2015) 200–203, letter, https://doi.org/10.1038/nature14674.
[11] S. Wang, Z. Shan, H. Huang, The mechanical properties of nanowires, Adv. Sci. 4 (4) (2017) 1600332–n/a, 1600332, https://doi.org/10.1002/advs.201600332.
[12] Q. Zhang, Q.-K. Li, M. Li, Chemical segregation in metallic glass nanowires, J. Chem. Phys. 141 (19) (2014) 194701, https://doi.org/10.1063/1.4901739.
[13] Editorial, Crystallizing glassy issues, Nat. Mater. 14 (June) (2015) 541–541, http://www.nature.com/doifinder/10.1038/nmat4319.
[14] D.J. Magagnosc, W. Chen, G. Kumar, J. Schroers, D.S. Gianola, Thermomechanical behavior of molded metallic glass nanowires, Sci. Rep. 6 (2016) 19530 EP, https://doi.org/10.1038/srep19530.
[15] D. Şopu, A. Foroughi, M. Stoica, J. Eckert, Brittle-to-ductile transition in metallic glass nanowires, Nano Lett. 16 (7) (2016) 4467–4471, pMID: 27248329, https://doi.org/10.1021/acs.nanolett.6b01636.
[16] Q. Zhang, Q.-K. Li, M. Li, Key factors affecting mechanical behavior of metallic glass nanowires, Sci. Rep. 7 (2017) 41365, https://doi.org/10.1038/srep41365. http://www.ncbi.nlm.nih.gov/pmc/articles/PMC5278411/.
[17] H. Guo, P.F. Yan, Y.B. Wang, J. Tan, Z.F. Zhang, M.L. Sui, E. Ma, Tensile ductility and necking of metallic glass, Nat. Mater. 6 (10) (2007) 735–739, https://doi.org/10.1038/nmat1984.
[18] J. Wachter, G. Gutiérrez, A. Zúñiga, R. Palma, Buckling of cu–zr-based metallic glasses nanowires: molecular dynamics study of surface effects, J. Mater. Sci. 49 (23) (2014) 8051–8056, https://doi.org/10.1007/s10853-014-8512-9.
[19] K. Albe, Y. Ritter, D. Şopu, Enhancing the plasticity of metallic glasses: shear band formation, nanocomposites and nanoglasses investigated by molecular dynamics simulations, Mech. Mater. 67 (Suppl. C) (2013) 94–103, nanostructured Materials, https://doi.org/10.1016/j.mechmat.2013.06.004.
[20] V.K. Sutrakar, D.R. Mahapatra, Stress-induced martensitic phase transformation in cuzr nanowires, Mater. Lett. 63 (15) (2009) 1289–1292, https://doi.org/10.1016/j.matlet.2009.02.064.
[21] M.I. Mendelev, M.J. Kramer, R.T. Ott, D.J. Sordelet, D. Yagodin, P. Popel, Development of suitable interatomic potentials for simulation of liquid and amorphous cu-zr alloys, Philos. Mag. 89 (11) (2009) 967–987, 435YYTimes Cited:0Cited References Count:33, https://doi.org/10.1080/14786430902832773Pii910503793, http://000265380600003.
[22] Q. Cheng, H.A. Wu, Y. Wang, X.X. Wang, Pseudoelasticity of cuzr nanowires via stress-induced martensitic phase transformations, Appl. Phys. Lett. 95 (2) (2009), http://scitation.aip.org/content/aip/journal/apl/95/2/10.1063/1.3183584.
[23] C. Wang, C. Wong, Structural properties of zrxcu90xal10 metallic glasses investigated by molecular dynamics simulations, J. Alloys Compd. 510 (1) (2012) 107–113, https://doi.org/10.1016/j.jallcom.2011.07.110.
[24] S. Melchionna, G. Ciccotti, B. Lee Holian, Hoover npt dynamics for systems varying in shape and size, Mol. Phys. 78 (3) (1993) 533–544, https://doi.org/10.1080/00268979300100371.

[25] M. Sepúlveda-Macías, N. Amigo, G. Gutiérrez, On set of plasticity and its relation to atomic structure in cuzr metallic glass nanowire: a molecular dynamics study, J. Alloys Compd. 655 (2016) 357–363, https://doi.org/10.1016/j.jallcom.2015.09.149.
[26] S. Plimpton, Fast parallel algorithms for short-range molecular dynamics, J. Comput. Phys. 117 (1) (1995) 1–19, https://doi.org/10.1006/jcph.1995.1039.
[27] F. Shimizu, S. Ogata, J. Li, Theory of shear banding in metallic glasses and molecular dynamics calculations, Mater. Trans. 48 (11) (2007) 2923–2927.
[28] A. Stukowski, Visualization and analysis of atomistic simulation data with ovito the open visualization tool, Model. Simul. Mater. Sci. Eng. 18 (1) (2010) 015012, http://stacks.iop.org/0965-0393/18/i=1/a=015012.
[29] K. Song, S. Pauly, Y. Zhang, R. Li, S. Gorantla, N. Narayanan, U. Kühn, T. Gemming, J. Eckert, Triple yielding and deformation mechanisms in metastable cu47.5zr47.5al5 composites, Acta Mater. 60 (17) (2012) 6000–6012, https://doi.org/10.1016/j.actamat.2012.07.015.
[30] K.K. Song, S. Pauly, B.A. Sun, J. Tan, M. Stoica, U. Kühn, J. Eckert, Correlation between the microstructures and the deformation mechanisms of cuzr-based bulk metallic glass composites, AIP Adv. 3 (1) (2013) 012116, https://doi.org/10.1063/1.4789516.
[31] F. Wu, K. Chan, S. Chen, S. Jiang, G. Wang, Zr cu-based bulk metallic glass composites with large strain-hardening capability, Mater. Sci. Eng. A 636 (2015) 502–506, https://doi.org/10.1016/j.msea.2015.04.027.
[32] D. Şopu, M. Stoica, J. Eckert, Deformation behavior of metallic glass composites reinforced with shape memory nanowires studied via molecular dynamics simulations, Appl. Phys. Lett. 106 (21) (2015) 211902, https://doi.org/10.1063/1.4921857.
[33] T. Brink, M. Peterlechner, H. Rösner, K. Albe, G. Wilde, Influence of crystalline nanoprecipitates on shear-band propagation in cu-zr-based metallic glasses, Phys. Rev. Appl. 5 (2016) 054005, https://doi.org/10.1103/PhysRevApplied.5.054005.
[34] N. Amigo, M. Sepulveda-Macias, G. Gutierrez, Martensitic transformation to monoclinic phase in bulk b2cuzr, Intermetallics 91 (Suppl. C) (2017) 16–21, https://doi.org/10.1016/j.intermet.2017.08.003.
[35] M.I. Mendelev, D.J. Sordelet, M.J. Kramer, Using atomistic computer simulations to analyze x-ray diffraction data from metallic glasses, J. Appl. Phys. 102 (4) (2007), https://doi.org/10.1063/1.2769157.
[36] Y. Wu, D.Q. Zhou, W.L. Song, H. Wang, Z.Y. Zhang, D. Ma, X.L. Wang, Z.P. Lu, Ductilizing bulk metallic glass composite by tailoring stacking fault energy, Phys. Rev. Lett. 109 (2012) 245506, https://doi.org/10.1103/PhysRevLett.109.245506.
[37] S. Feng, L. Qi, L. Wang, P. Yu, S. Zhang, M. Ma, X. Zhang, Q. Jing, K. Ngai, A. Greer, G. Li, R. Liu, Structural feature of cu64zr36 metallic glass on nanoscale: densely-packed clusters with loosely-packed surroundings, Scr. Mater. 115 (2016) 57–61, https://doi.org/10.1016/j.scriptamat.2015.12.038.
[38] H.W. Sheng, W.K. Luo, F.M. Alamgir, J.M. Bai, E. Ma, Atomic packing and short-to-medium-range order in metallic glasses, Nature 439 (7075) (2006) 419–425, https://doi.org/10.1038/nature04421.
[39] A. Hirata, P. Guan, T. Fujita, Y. Hirotsu, A. Inoue, A.R. Yavari, T. Sakurai, M. Chen, Direct observation of local atomic order in a metallic glass, Nat. Mater. 10 (1) (2011) 28–33, https://doi.org/10.1038/nmat2897.
[40] Y.Q. Cheng, A.J. Cao, E. Ma, Correlation between the elastic modulus and the intrinsic plastic behavior of metallic glasses: the roles of atomic configuration and alloy composition, Acta Mater. 57 (11) (2009) 3253–3267, https://doi.org/10.1016/j.actamat.2009.03.027.
[41] Y. Sun, B. Wei, Y. Wang, W. Li, C. Shek, Enhanced plasticity of zr-based bulk metallic glass matrix composite with ductile reinforcement, J. Mater. Res. 20 (2005) 2386–2390, https://doi.org/10.1557/jmr.2005.0320. http://journals.cambridge.org/article_S0884291400091561.